Loss of synaptic ribbons is an early cause in ROS-induced acquired sensorineural hearing loss

Kurasawa, Shunkou
Mohri, Hiroaki
Tabuchi, Keiji
Ueyama, Takehiko

(Citation)
Neurobiology of Disease,186:106280

(Issue Date)
2023-10-01

(Resource Type)
journal article

(Version)
Version of Record

Neurobiology of Disease 186 (2023) 106280

Contents lists available at ScienceDirect

Neurobiology of Disease

journal homepage: www.elsevier.com/locate/ynbdi

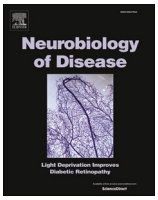

Loss of synaptic ribbons is an early cause in ROS-induced acquired sensorineural hearing loss

Shunkou Kurasawa [a,b], Hiroaki Mohri [a], Keiji Tabuchi [b], Takehiko Ueyama [a,*]

[a] Laboratory of Molecular Pharmacology, Biosignal Research Center, Kobe University, Kobe 657-8501, Japan
[b] Department of Otolaryngology-Head and Neck Surgery, University of Tsukuba, Tsukuba 300-8575, Japan

ARTICLE INFO

Keywords:
Aging
Cisplatin
Cochlear hair cell
Cochlear synaptopathy
CtBP2
Hidden hearing loss
NADPH oxidase
Noise
Piccolo 1
Ribbon synapse

ABSTRACT

Considerable evidence of reactive oxygen species (ROS) involvement in cochlear hair cell (HC) loss, leading to acquired sensorineural hearing loss (SNHL), were reported. Cochlear synaptopathy between HCs and spiral ganglion neurons has been gathering attention as a cochlear HC loss precursor not detectable by normal auditory evaluation. However, the molecular mechanisms linking ROS with HC loss, as well as the relationship between ROS and cochlear synaptopathy have not been elucidated. Here, we examined these linkages using *NOX4*-TG mice, which constitutively produce ROS without stimulation. mRNA levels of Piccolo 1, a major component of the synaptic ribbon (a specialized structure surrounded by synaptic vesicles in HCs), were decreased in postnatal day 6 *NOX4*-TG mice cochleae compared to those in WT mice; they were also decreased by noise exposure in 2-week-old WT cochleae. As noise exposure induces ROS production, this suggests that the synaptic ribbon is a target of ROS. The level of CtBP2, another synaptic ribbon component, was significantly lower in *NOX4*-TG cochleae of 1-month-old and 4-month-old mice compared to that in WT mice, although no significant differences were noted at 1.5- and 2-months. The decrease in CtBP2 plateaued in 4-month-old *NOX4*-TG, while it gradually decreased from 1 to 6 months in WT mice. Furthermore, CtBP2 level in 2-month-old *NOX4*-TG mice decreased significantly after exposure to cisplatin and noise compared to that in WT mice. These findings suggest that ROS lead to developmental delays and early degeneration of synaptic ribbons, which could be potential targets for novel therapeutics for ROS-induced SNHL.

1. Introduction

Reactive oxygen species (ROS) are known to play key roles in numerous physiological and pathological processes (Leto et al., 2009). Although appropriate ROS levels are indispensable for cell survival and differentiation (Leto et al., 2009), higher levels induce oxidative stress, including in the inner ear and central nervous system (CNS). This can trigger pathologies such as sensorineural hearing loss (SNHL), as well as CNS injury and neurodegeneration (Ma et al., 2017; Yang et al., 2015).

Hearing loss is one of the most common sensory deficits in humans (Muller and Barr-Gillespie, 2015); however, effective pharmacological interventions targeting specific molecules have not yet been developed (Muller and Barr-Gillespie, 2015). The cochlea contains two types of hair cells (HCs)—inner HCs (IHCs) and outer HCs (OHCs). IHCs are true sensors, whereas OHCs are responsible for the mechanical amplification process that leads to high sensitivity and fine frequency resolution. The cochlea has a tonotopic gradient along the length of the lumen; the basal turn detects high-frequency sounds, whereas the apical turn detects low-frequency sounds (Goutman et al., 2015).

SNHL was considered to result from cell death, including HC death in the cochlea; however, it has recently been demonstrated that "hidden hearing loss" can be caused by damage to the ribbon synapses between HCs and spiral ganglion neurons but without HC loss (Wei et al., 2020; Wu et al., 2020). The damage/loss of ribbon synapses in cochleae, called "cochlear synaptopathy", is not evidenced in clinical audiological tests (such as the auditory brainstem response [ABR] and distortion product

Abbreviations: ABR, auditory brainstem response; ANOVA, analysis of variance; ARHL, age-related hearing loss; CNS, central nervous system; DAPI, 4′,6-diamidino-2-phenylindole; DIHL, drug-induced hearing loss; DPOAE, distortion product otoacoustic emission; GAPDH, glyceraldehyde 3-phosphate dehydrogenase; HC, hair cell; IHC, inner hair cell; NIHL, noise-induced hearing loss; NOX, NADPH oxidase; OC, organ of Corti; OHC, outer hair cell; PBS, phosphate-buffered saline; ROS, reactive oxygen species; SNHL, sensorineural hearing loss; SPL, sound pressure level; SV, synaptic vesicles; TG, transgenic.

* Corresponding author at: 1-1 Rokkodai-cho, Nada-ku, Kobe 657-8501, Japan.
E-mail address: tueyama@kobe-u.ac.jp (T. Ueyama).

https://doi.org/10.1016/j.nbd.2023.106280
Received 13 August 2023; Received in revised form 1 September 2023; Accepted 1 September 2023
Available online 4 September 2023

otoacoustic emission [DPOAE] tests) and can result in speech-in-noise difficulties, tinnitus, and/or hyperacusis (Aedo and Aguilar, 2020). Nevertheless, although threshold sensitivity as measured by the ABR and DPOAE tests is normal, a reduced ABR wave I amplitude may be detected in cases of "cochlear synaptopathy" and "hidden hearing loss" (Hickox et al., 2017; Kujawa and Liberman, 2009). The presynaptic (synaptic) ribbon is a specialized structure found on the presynaptic side of the sensory synapse in HCs and photoreceptors to connect with postsynaptic neurons via neurotransmission (Kantardzhieva et al., 2012). It is composed of Piccolo; C-terminal-binding protein 2 (CtBP2), a transcriptional co-repressor that contains a B-domain; RIBEYE, a splice variant of CtBP2 that comprises a unique A-domain and the B-domain; Bassoon (Schmitz, 2009); and surrounding and tethering synaptic vesicles (SV; Fig. 1A), and enables rapid and sustained signal transmission (Kantardzhieva et al., 2012).

Previous studies have convincingly argued that ROS contribute to the development of the acquired SNHL triad—that is, age-related hearing loss (ARHL), noise-induced hearing loss (NIHL), and drug-induced hearing loss (DIHL) (Yang et al., 2015). Recently, we established a mouse model of ROS overproduction in cochleae by creating transgenic (TG) mice that express the gene for human NADPH oxidase (NOX) 4 (*NOX4*-TG mice). These mice produce low levels of ROS without stimulation and exhibit hearing vulnerability after noise exposure despite having normal hearing function under baseline conditions (Morioka et al., 2018), confirming that ROS contribute to NIHL. Although NOX3 is the main NOX that contributes to acquired SNHL (Mohri et al., 2021; Mukherjea et al., 2010), the expression of NOX4 in the cochlea (Liu et al., 2021; Rousset et al., 2020) and its contribution to SNHL (Liu et al., 2021) has recently been reported. Moreover, antioxidant supplementation in animals and humans has been reported to prevent progression of ARHL and NIHL (Chen et al., 2020; Tavanai and Mohammadkhani, 2017).

Although we have previously reported the mechanism of HC loss by induced NOX3 expression in OHCs and supporting cells in aging, after noise exposure, and administration of cisplatin (Mohri et al., 2021), the underlying molecular mechanism of HC loss due to ROS remains unknown. The present study aimed to evaluate the effects of ROS on the synaptic ribbon using *NOX4*-TG mice.

2. Materials and methods

2.1. Mice and anesthesia

This study was approved by the Institutional Animal Care and Use Committee of Kobe University (approval nos. 26–03-05 and 2020-06-04) and carried out according to the Kobe University Animal Experimentation Regulations. *NOX4*-TG mice, which have 17 copies of the transgene *CAG promoter;3xFLAG-NOX4;polyA* integrated into the genome, were generated as previously described (Morioka et al., 2018). All mice were identified using numbered ear tags, and housed (maximum 5 in a cage) under specific pathogen-free conditions using an individually ventilated cage system (Techniplast, Tokyo, Japan) with ad libitum access to food and water. The animal facility was maintained on a 14 h light and 10 h dark cycle at 23 ± 2 °C and 50 ± 10% humidity. Both male and female mice were used in the present study (mice <4-week-old were not differentiated based on sex; average weights of P6, P14–15, 6-week-old, and 2-month-old mice were 3.5–5.0, 6.0–8.0, 15–20, 18.5–24 g, respectively). Age- and sex-matched WT siblings were used as controls of *NOX4*-TG mice. To minimize pain and to obtain long effects in mice, we chose a mixed anesthesia. Mice were anesthetized (for ABR measurement, noise exposure experiment, and perfusion fixation) using a mixture of 0.3 mg/kg medetomidine, 4.0 mg/kg midazolam, and 5.0 mg/kg butorphanol administered by intraperitoneal injection. Mice were sacrificed (for DNA microarray and immunoblotting) by overanesthesia (120 mg/kg pentobarbital by intraperitoneal injection) followed by decapitation.

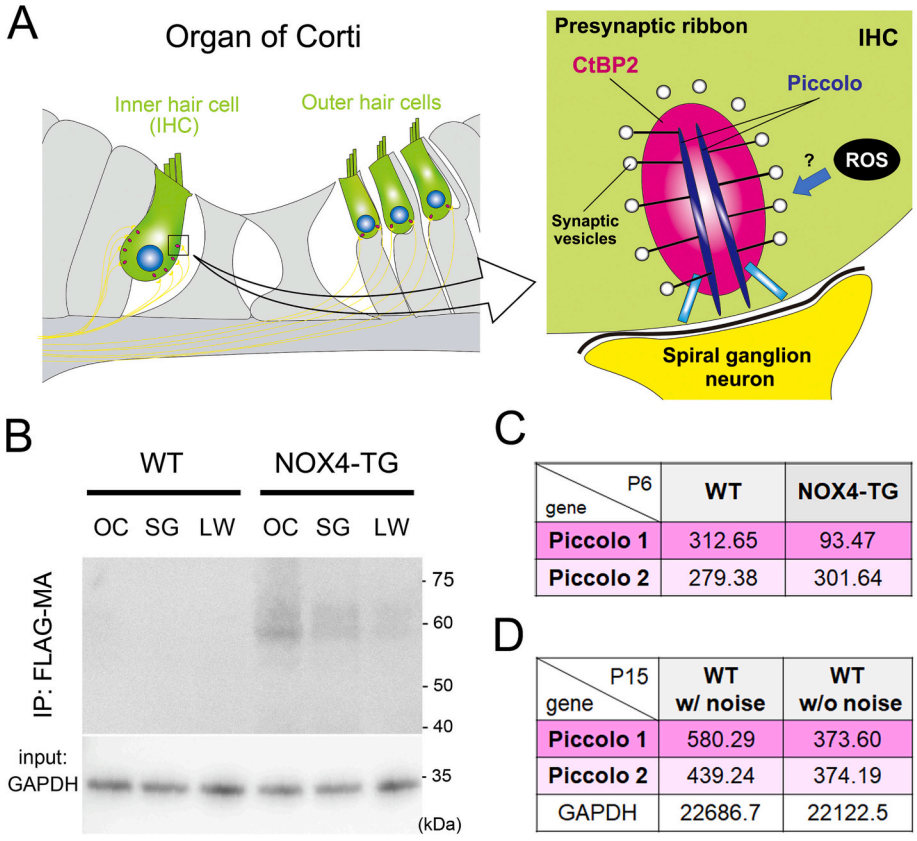

C

P6 gene	WT	NOX4-TG
Piccolo 1	312.65	93.47
Piccolo 2	279.38	301.64

D

P15 gene	WT w/ noise	WT w/o noise
Piccolo 1	580.29	373.60
Piccolo 2	439.24	374.19
GAPDH	22686.7	22122.5

Fig. 1. Piccolo is a target of reactive oxygen species (ROS) and noise exposure.
A. The left panel shows a single row of inner hair cells (IHCs) and three rows of outer hair cells (OHCs) in the organ of Corti (OC). The right panel shows a magnified view of the ribbon synapse between an IHC and a spiral ganglion neuron of the cochlear nerve (indicated within the square in the left panel). Piccolo and CtBP2 are the main components of the presynaptic ribbon.
B. Lysates were prepared from the OC, spiral ganglion, and lateral wall of WT and *NOX4*-TG cochleae. Equal amounts of protein were immunoprecipitated using a magnetic agarose (MA)-conjugated FLAG antibody followed by SDS-PAGE, then immunoblotted using an HRP-conjugated FLAG antibody. Comparable loading of proteins was confirmed by GAPDH immunoblotting.
C and D. Total RNA was obtained from WT and *NOX4*-TG cochleae at P6 (C) and from WT cochleae with or without noise exposure at P15 (D). DNA microarray analysis results focused on Piccolo 1 and Piccolo 2 are shown.

2.2. Antibodies

The following specific antibodies were used: CtBP2 monoclonal antibody (BD Biosciences, cat# 612044, RRID:AB_399431; 1:200) and myosin-VIIa polyclonal antibody (Proteus Biosciences, cat# 25–6790, RRID:AB_10015251; 1:500). Magnetic agarose-conjugated FLAG (cat# M185-10R), horseradish peroxidase (HRP)-conjugated FLAG (cat# M185–7; RRID:AB_2687978), and HRP-conjugated glyceraldehyde 3-phosphate dehydrogenase (GAPDH) (cat# M171–7; RRID:AB_10699462; 1:2000) monoclonal antibodies were purchased from MBL (Nagoya, Japan). Alexa Fluor 488-labeled anti-rabbit IgG (RRID: AB_143165; 1:500) and Alexa Fluor 594-labeled anti-mouse IgG (RRID: AB_2534087; 1:500) antibodies were purchased from Thermo Fisher Scientific (Thermo Fisher Scientific, Waltham, MA, USA).

2.3. Immunoprecipitation and immunoblotting

The cochleae of P6 WT and *NOX4*-TG mice were dissected into three parts (OC, spiral ganglion, and lateral wall) and lysed in homogenizing buffer (Morioka et al., 2020; Ueyama et al., 2016) by sonication in the presence of protease and protein phosphatase inhibitor cocktails (Nacalai Tesque, Japan; cat# 03969–21) and 1% Triton X-100. Total lysates were centrifuged at 900*g* at 5 min at 4 °C, and the protein concentration of supernatant samples was determined using a BCA protein assay kit (Thermo Fisher Scientific). Equal amounts of proteins were incubated with 5 μl magnetic agarose-conjugated FLAG antibody for 12 h at 4 °C. After washing with PBS containing 0.3% Tween-20, the eluted proteins were subjected to SDS-PAGE (5–20% gradient gels, Fujifilm Wako Pure Chemical, Osaka Japan) and transferred on to PVDF membranes. The membranes were immunoblotted using an HRP-conjugated FLAG antibody, followed by detection using an enhanced chemiluminescence detection system (Clarity; Bio-Rad Laboratories, Hercules, CA, USA). Comparable protein loading was confirmed by immunoblotting using an HRP-conjugated antibody against GAPDH.

2.4. DNA microarray analysis

DNA microarray analysis was performed as previously described (Ueyama et al., 2020). Total RNA was extracted from the cochleae of the two experimental pairs (five each WT vs. *NOX4*-TG mice at P6 and four each WT mice without noise exposure vs. WT mice with noise exposure at P15 [24 h after noise exposure]) using a NucleoSpin RNA kit (MACHEREY-NAGEL GmbH & Co. KG, Düren, Germany; cat# 740955). Gene expression profiles were examined using the SurePrint G3 Mouse GE 8 × 60 K Microarray Kit (Agilent Technologies, Santa Clara, CA, USA).

2.5. ABR measurement

ABR measurements were performed as previously reported (Mohri et al., 2021). Briefly, mice were anesthetized and electroencephalographic recording was performed using BioSigRP software and the TDT System 3 (Tucker-Davis Technologies, Alachua, FL, USA) to generate clicks or tone-burst stimulation at 8, 16, 24, 32, and 48 kHz. Waveforms from 500 stimuli were averaged, and ABR thresholds were estimated by decreasing the sound intensity in 5 dB steps from 90 dB SPL until the lowest sound intensity level was reached resulting in a recognizable ABR wave pattern (judged by the recognition of wave III). When there was no response to stimulation at 90 dB, the threshold was considered to be 100 dB. The experiments were terminated if the mice showed signs of unbearable pain.

2.6. Cisplatin treatment

For the cisplatin insult experiments, cisplatin (5 mg/kg) was administered intraperitoneally to 2-month-old WT and *NOX4*-TG mice for six consecutive days (Fig. 5A). ABR was assessed twice: before cisplatin treatment on day 0 and before fixation on day 7. We set the endpoint of the experiments, which was defined as a decrease of >1/4 the body weight at day 4 with daily body weight measurements. The number of remaining OHCs and IHCs as well as the number of CtBP2 dots in IHCs were evaluated at 180° in the apical turn, 270° in the middle turn, and 420° (CtBP2) or 450° (OHC) in the basal turn of the cochlea. ABR and counts for HC loss and CtBP2 were performed on both sides, and the average of both sides was used for evaluation.

2.7. Noise exposure

Noise exposure experiments were performed as previously described (Morioka et al., 2018). Anesthetized P14 WT mice were exposed to 110 dB SPL of octave-band noise centered at 8 kHz for 1 h inside a sound chamber. To ensure the uniformity of the stimulus, we calibrated and measured the sound levels using a sound level meter (NL-26: RION, Tokyo, Japan) positioned at the level of the animal's head. Twenty-four hours after noise exposure (P15), total RNA was extracted from four mice with or without noise exposure each. At 2 months of age, anesthetized female WT and *NOX4*-TG mice were exposed to 110 dB SPL noise for 75 min. ABR was assessed immediately before noise exposure, then sequentially immediately after noise exposure (on day 0) and on days 3 and 7 after noise exposure (Fig. 6A). During the experiments, the mice were observed through a small window in the sound chamber, and the experiments were terminated if they showed signs of unbearable pain. The number of remaining OHCs and IHCs as well as the number of CtBP2 dots in IHCs were evaluated at 180° in the apical turn, 270° in the middle turn, and 390°, 450°, and 510° in the basal turn of the cochlea. ABR and counts for HC loss and CtBP2 were performed on both sides, and the average of both sides was used for evaluation.

2.8. Immunohistochemistry

To examine surface preparations of cochleae, anesthetized mice were transcardially fixed with 4% paraformaldehyde in 0.1 M phosphate buffer (pH 7.4), and the dissected inner ears were decalcified in 0.12 M EDTA for 2 days at 23 °C (Ueyama et al., 2014). After permeabilization with PBS containing 0.3% Tween-20, fixed cochleae were incubated with monoclonal anti-CtBP2 and polyclonal anti-myosin-VIIa antibodies for 12 h at 4 °C, and then with Alexa Fluor 488-labeled and Alexa Fluor 594-labeled secondary antibodies and 4′,6-diamidino-2-phenylindole (DAPI) as the nuclear counterstain for 45 min at 23 °C. In some cases, Alexa Fluor 488-labeled phalloidin (Thermo Fisher Scientific, cat# A12379; 1: 750) was used instead of myosin-VIIa staining. Stained tissues were mounted in ProLong Antifade (Thermo Fisher Scientific) and imaged using a confocal microscope (LSM900; Carl Zeiss, Oberkochen, Germany) with an oil-immersion 63× (or 40×) objective. Each image contained 8–15 IHCs and 30–50 (or 55–70) OHCs stacked at 1.0 μm intervals, with the span adjusted to include all synaptic ribbons. Maximum intensity projection images were obtained from each z-stack image using ZEN software (Carl Zeiss). CtBP2 dots and HCs were counted at 180° in the apical turn, 270° in the middle turn, and 390°, 450°, and 510° in the basal turn of the cochlea in noise exposure experiments. For cisplatin experiments, these quantities were counted at 180°, 270°, and 420° (CtBP2) or 450° (HCs) (Fig. 2A). CtBP2-positive synaptic ribbons in IHCs were counted, and the average number of ribbons per 10 IHCs was calculated for each location of the cochlea. For remaining OHCs and IHCs, myosin-VIIa-positive cells or phalloidin-positive cells with stereocilia in the above-mentioned regions were counted (data presented as percentages).

2.9. Statistical analysis

The exact numbers of experiments for each condition are mentioned in the corresponding figures or figure legends. All data are presented as

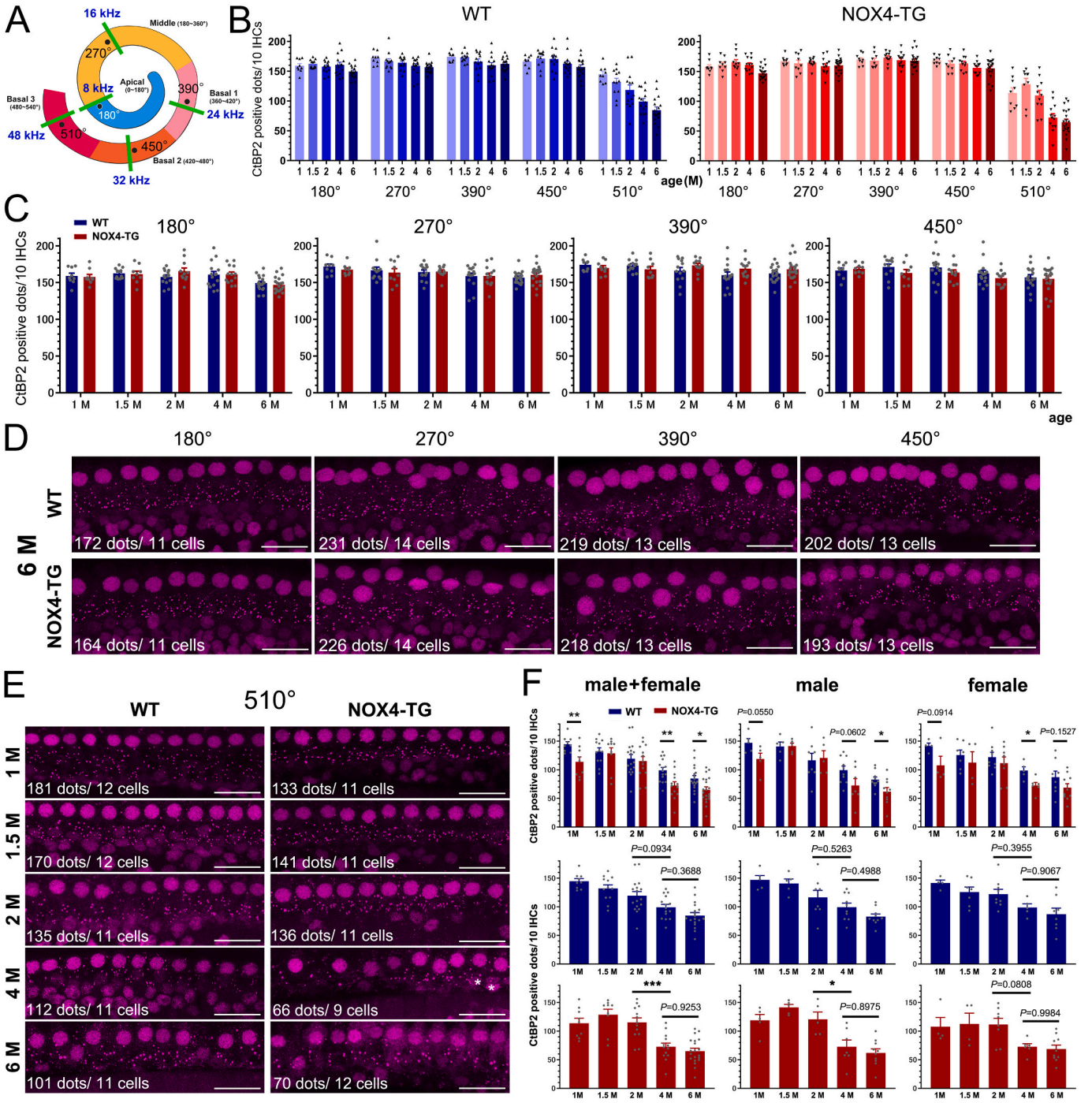

Fig. 2. Time course of the CtBP2 number in WT and *NOX4*-TG cochleae.

A. Illustration showing the three regions (apical, middle, and basal turns), and corresponding degrees (°) and frequencies (8–48 kHz), of the cochlea.

B-C. Graphs (left; WT, right; *NOX4*-TG) showing the number of CtBP2 positive dots/10 IHCs at 180°, 270°, 390°, 450°, and 510° of the cochlea at 1, 1.5, 2, 4, and 6 months (M) of age (B). Graphs showing a comparison of the CtBP2-positive dot number at 180°, 270°, 390°, and 450° between WT and *NOX4*-TG mice (C). The dots in the graphs indicate the number of male and female mice analyzed. No significant difference was noted between WT and *NOX4*-TG mice based on the Student's *t*-test.

D. Representative images of CtBP2 immunostaining in 6-month-old male WT and *NOX4*-TG mice cochleae at 180°, 270°, 390°, and 450°. Scale bars; 20 μm.

E. Representative images of CtBP2 immunostaining in male WT and *NOX4*-TG mice cochleae at 510° at 1, 1.5, 2, 4, and 6 months (M) of age. Asterisks, myosin-VIIa negative inner phalangeal cells; Scale bars, 20 μm.

F. Graphs showing the number of CtBP2 positive dots/10 IHCs at 510° between 1-, 1.5-, 2-, 4-, and 6-month-old WT and *NOX4*-TG mice. Graphs are shown for males and females, males alone, and females alone, focusing on the comparison between WT and *NOX4*-TG mice (upper panels) and time courses in WT (middle panels) and *NOX4*-TG (bottom panels) mice. The dots in the graphs indicate the number of mice analyzed ($n > 4$ in each group). Significant differences were assessed using Student's *t*-test (upper panels) or one-way ANOVA with Tukey's post-hoc test (middle and bottom panels). *P*-values are shown in the graphs. *, $P < 0.05$; **, $P < 0.01$.

the mean ± SEM values. Unpaired, two-tailed Student's *t*-tests were used for between-group comparisons. For comparisons between more than two groups, one-way or two-way analysis of variance (ANOVA) was used, followed by Tukey's post-hoc test for pairwise group differences. All statistical analyses were performed using GraphPad Prism 7.0 (GraphPad Software Inc., San Diego, CA, USA), and significant differences are indicated by *, $P < 0.05$; **, $P < 0.01$; ***, $P < 0.001$; and ****, $P < 0.0001$.

3. Results

3.1. Decreased Piccolo mRNA levels in NOX4-TG mice as well as in WT mice with noise exposure

First, we confirmed the expression of FLAG-NOX4 in the inner ear using immunoblotting. FLAG-NOX4 was found to be expressed in the organ of Corti (OC), spiral ganglion, and lateral wall of the cochleae of postnatal day 6 (P6) *NOX4*-TG mice, but not WT mice (Fig. 1B and Fig. S1, uncropped images); this was consistent with our previous data showing that ROS production in cochleae (at P7) and the levels of 4-hydroxy-2-nonenal, a marker for lipid peroxidation, in the OC and the lateral wall (at P14) were higher in *NOX4*-TG mice compared to those in WT mice (Morioka et al., 2018). Here, we additionally demonstrated FLAG-NOX4 expression in the spiral ganglion neurons (Fig. 1B).

To screen for genes that were upregulated or downregulated more than two-fold in the cochleae of P6 *NOX4*-TG mice relative to those in WT mice, DNA microarray analysis was used. Among these genes, we focused on Piccolo, which is a major component of the synaptic ribbon in presynaptic cochlear HCs. The ratio (*NOX4*-TG/WT) of *Piccolo 1* mRNA in the cochlea was 0.299 (93.47/321.65), whereas that of *Piccolo 2*, a shorter, alternative splicing variant with a distinct C-terminus, was 1.080 (301.64/279.38) (Fig. 1C).

To examine the involvement of Piccolo in ROS-induced SNHL, WT mice were exposed to intense noise known to induce ROS production (Kurabi et al., 2017) at the age of 2 weeks, when anatomical features of HCs and hearing function as evaluated based on the ABR mature (Krey et al., 2020; Narui et al., 2009). Although the ratio (after noise exposure /before noise exposure) was decreased for both *Piccolo 1* and *2* mRNA, the decreased ratio was more apparent for the former (*Piccolo 1*: 373.60/580.29 [0.644], *Piccolo 2*: 374.19/439.24 [0.852]) (Fig. 1D).

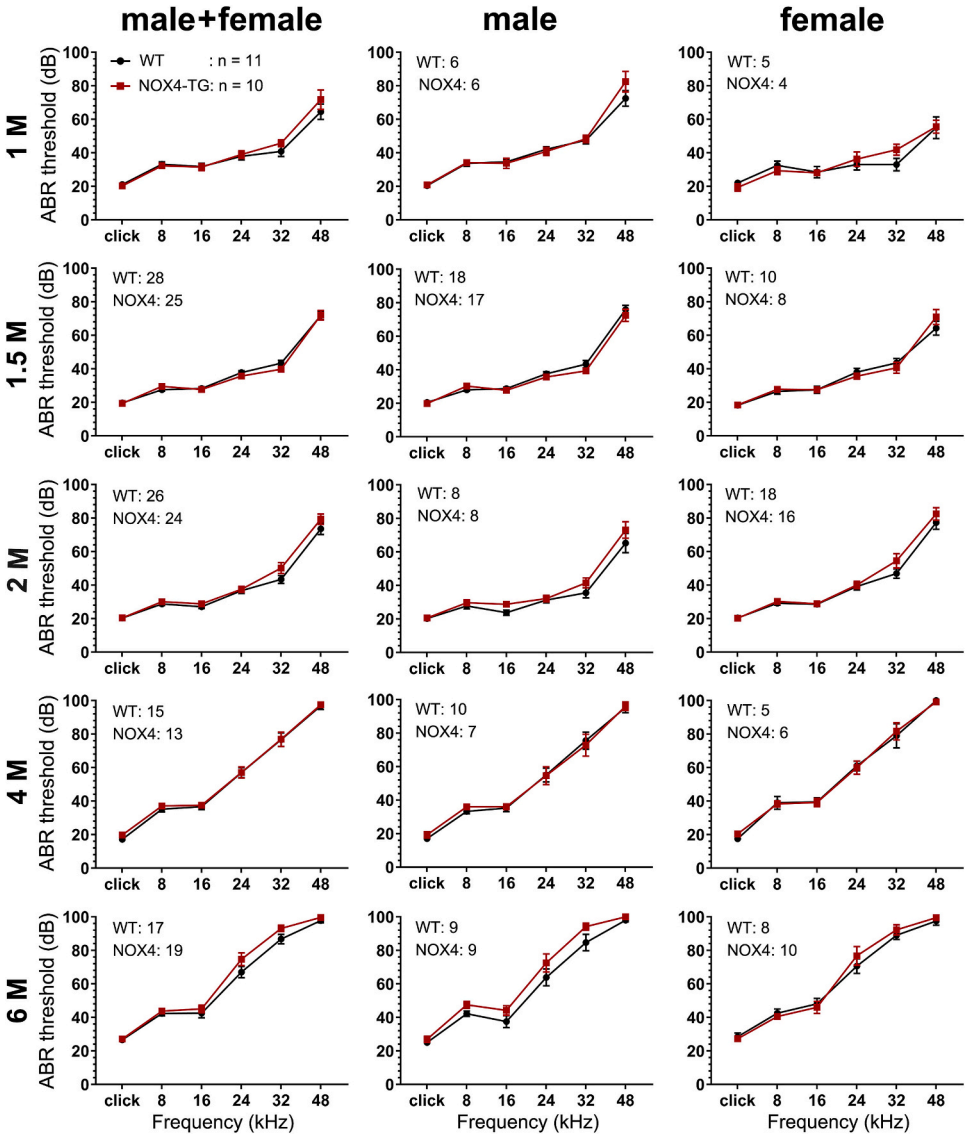

Fig. 3. Time course of ABR threshold in WT and *NOX4*-TG mice.
ABR thresholds of male and female, male, and female WT and *NOX4*-TG mice were evaluated at 1, 1.5, 2, 4, and 6 months (M) of age. No significant differences were detected using two-way ANOVA with Tukey's post-hoc test. The number of mice evaluated is shown in the graphs.

3.2. Significant decrease in synaptic ribbon number in aged NOX4-TG mice

Next, we examined the number of synaptic ribbons in IHCs at five locations (Fig. 2A; 180° in the apical turn; 270° in the middle turn; and 390°, 450°, and 510° in the basal turn) in 1-, 1.5-, 2-, 4-, and 6-month-old WT and *NOX4*-TG mice. CtBP2 immunostaining had to be used for this purpose because of the lack of commercially available anti-Piccolo 1 and Bassoon antibodies suitable for immunohistological evaluation. Although no significant differences were observed at 180°, 270°, 390°, or 450° between WT and *NOX4*-TG cochleae at all time points (1 month to 6 months, Fig. 2B–D), a significant decrease in synaptic ribbon number at 510° was noted at 4 and 6 months in *NOX4*-TG cochleae compared to that in WT cochleae (Fig. 2B, E–F). Interestingly, the decrease in synaptic ribbon number plateaued after 4 months in *NOX4*-TG, but not in WT, mice (Fig. 2F). Similar data were obtained from the analyses of both male and female mice, males alone, and females alone (Fig. 2F). Additionally, the number of synaptic ribbons was significantly lower in *NOX4*-TG mice than in WT mice at 1 month, but not at 1.5 months. Considering the decrease in synaptic ribbon components (Piccolo 1 mRNA at P6 and CtBP2 protein at 1 month and after 4 months) in *NOX4*-TG mice, ROS may be involved in both developmental delay and early degeneration of synaptic ribbons/ribbon synapses.

3.3. Hearing function of NOX4-TG mice

Hearing function evaluated based on the ABR threshold was not significantly different between WT and *NOX4*-TG mice (in males and females, males alone, and females alone), but it tended to be worse in 6-month-old *NOX4*-TG mice than WT mice, especially in males (Fig. 3). To evaluate the relationships among hearing function, synaptic ribbons, and HC loss, we examined both OHC and IHC loss over time. OHC loss at

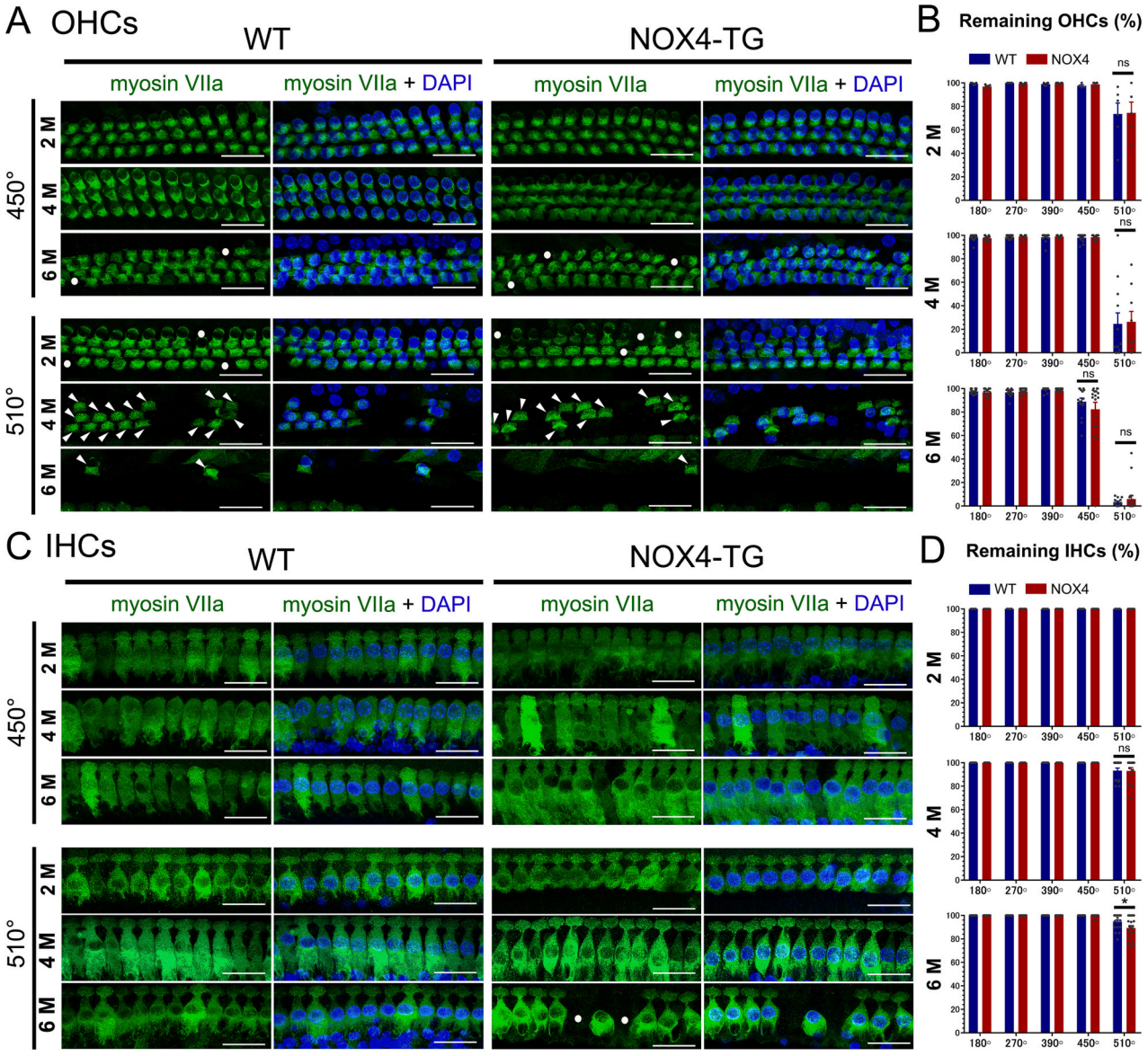

Fig. 4. Time course of HC (IHC and OHC) loss in WT and *NOX4*-TG mice.
A-D. WT and *NOX4*-TG cochleae were dissected at 2, 4, and 6 months (M) of age, and immunostained using a myosin-VIIa (green) antibody with DAPI (blue) counterstaining (A and C, males). Circles and arrowheads indicate HC loss and remaining OHCs, respectively. Scale bars; 20 μm. Remaining OHCs (B) and IHCs (D) at 180°, 270°, 390°, 450°, and 510° in the cochlea are graphed (males and females). The dots in the graphs show the number of mice analyzed (n > 4 in each group). Data for males and females are presented in Fig. S2. Student's *t*-test was used for the statistical analysis. *, $P < 0.05$; ns, not significant. (For interpretation of the references to colour in this figure legend, the reader is referred to the web version of this article.)

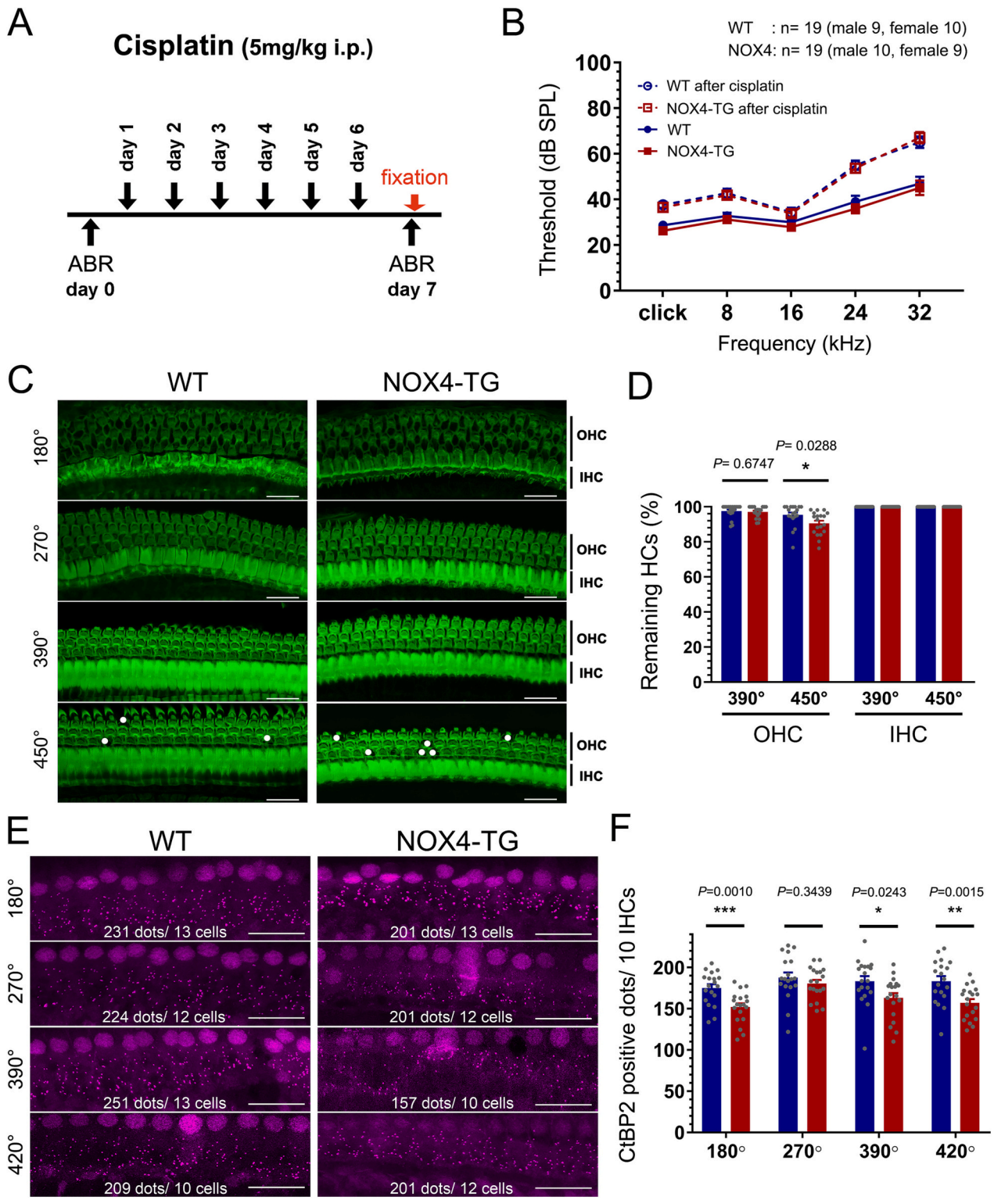

Fig. 5. Lower number of CtBP2 dots in 2-month-old *NOX4*-TG mice after cisplatin treatment.

Cisplatin treatment and ABR measurements were performed in 2-month-old WT (n = 19: male 9; female, 10) and *NOX4*-TG mice (n = 19: male, 10; female, 9).

A. Experimental protocol flowchart.

B. ABR thresholds before and after cisplatin treatment in WT and *NOX4*-TG mice. No significant differences were detected using two-way ANOVA with Tukey's post-hoc test.

C-F. Dissected cochleae of WT and *NOX4*-TG mice were stained with Alexa-488-conjugated phalloidin (green, C, 180° in the apical turn; 270° in the middle turn; 390° and 450° in the basal turn) and CtBP2 (magenta, E, 180° in the apical turn; 270° in the middle turn; 390° and 420° in the basal turn). Circles, HC loss; Scale bars, 20 μm. Remaining OHCs and IHCs (D) and CtBP2-positive dots/10 IHCs (F) are shown. Dots in the graphs indicate the number of mice analyzed. Student-*t*'s t-test was used for statistical analysis. P-value are shown in the graphs. *, $P < 0.05$; **, $P < 0.01$; ***, $P < 0.001$. (For interpretation of the references to colour in this figure legend, the reader is referred to the web version of this article.)

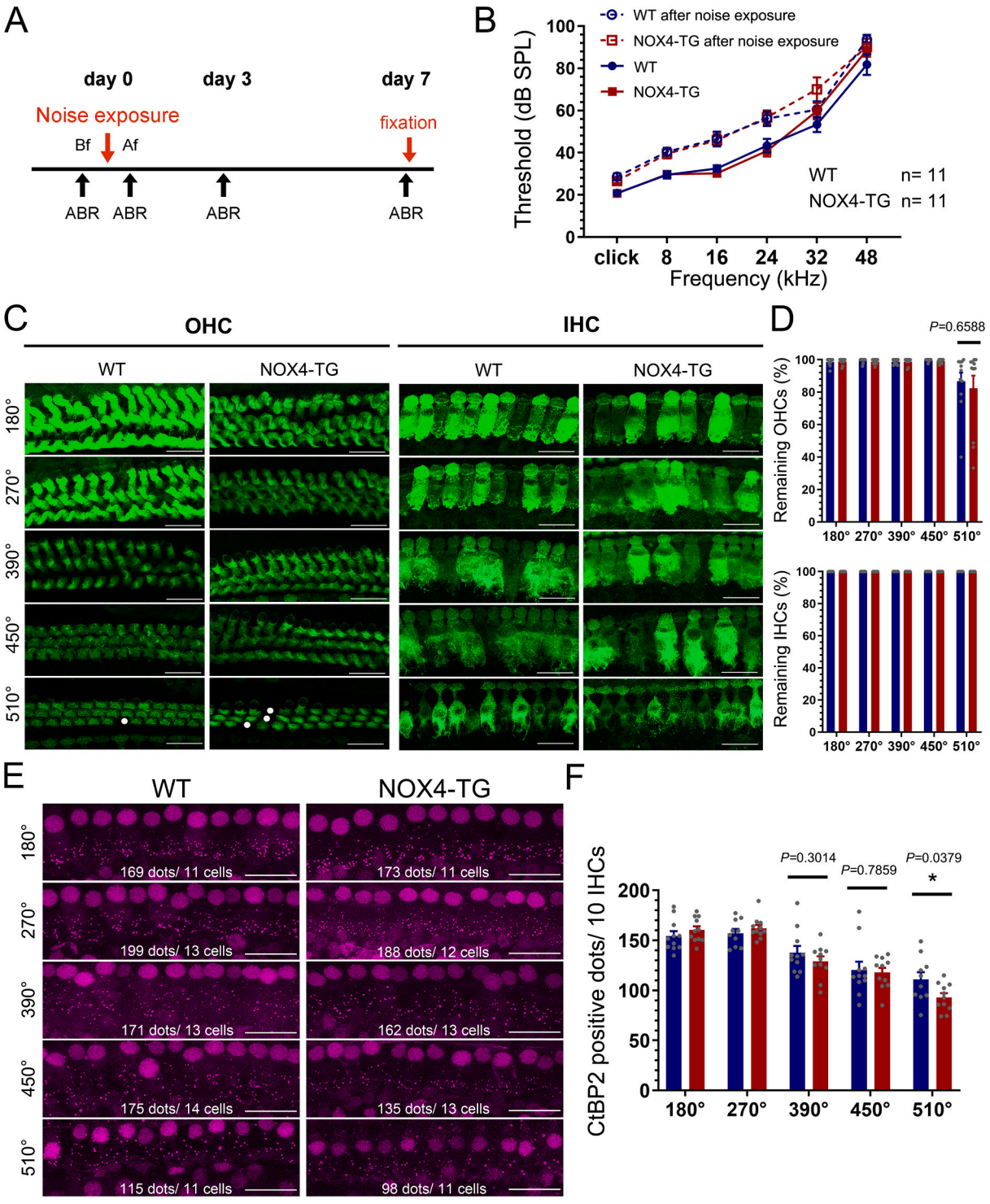

Fig. 6. Lower number of CtBP2 dots in 2-month-old *NOX4*-TG mice after noise exposure.
Noise exposure and ABR measurements were performed in 2-month-old female WT and *NOX4*-TG mice ($n = 11$, respectively).
A. Experimental protocol flowchart. Bf and Af, immediately before and after the noise exposure, respectively.
B. ABR thresholds before noise exposure on day 0 and after noise exposure on day 7 in WT and *NOX4*-TG mice. No significant differences were detected using two-way ANOVA with Tukey's post-hoc test. The ABR threshold shifts at day 0, 3, and 7 are presented in Fig. S3.
C-F. Dissected cochleae (at 180° in the apical turn, 270° in the middle turn, and 390°, 450°, and 510° in the basal turn) of WT and *NOX4*-TG mice were immunostained with myosin-VIIa (green, C) and CtBP2 (magenta, E). Remaining OHCs (D upper, n = 11) and IHCs (D lower, n = 11) and CtBP2 positive dots/10 IHCs (F; $n = 10$–11 [WT] and n = 11 [*NOX4*-TG]) are shown. Student-*t*'s t-test was used for the statistical analysis, and significant differences are indicated by * ($P < 0.05$). P-value are shown in the graphs. Circles, HC loss; Scale bars, 20 μm. (For interpretation of the references to colour in this figure legend, the reader is referred to the web version of this article.)

450° and 510° began occurring at 6 and 2 months, respectively (Fig. 4A–B), whereas IHC loss at 510° began occurring at 4 months (Fig. 4C–D). Similar data were obtained from analyses in male and female mice (Fig. 4), only males, and only females (Fig. S2). Although the difference in OHC loss between WT and *NOX4*-TG mice was not significant, IHC loss at 510° was statistically higher only in both male and female 6-month-old *NOX4*-TG mice compared to WT mice. Thus, a significant difference between WT and *NOX4*-TG mice may first be detected in the synaptic ribbons, followed by IHC loss, and finally, ABR. Reduced ABR wave I amplitude was not detected because there were no ABR waves at 48 kHz stimulation (corresponding to 510° in cochleae, see Fig. 2A) in almost all 4-month-old WT and *NOX4*-TG mice, but may be found in cochlear synaptopathy/hidden hearing loss (Hickox et al., 2017; Kujawa and Liberman, 2009).

3.4. Vulnerability of synaptic ribbons in NOX4-TG mice after cisplatin treatment

To examine whether the synaptic ribbon is a target of ROS-mediated acquired SNHL, we administered cisplatin, which induces ROS production in the cochlea (Ramkumar et al., 2021), to 2-month-old WT and *NOX4*-TG mice (Fig. 5A). Because it was difficult to obtain samples suitable for evaluating the basal turn of the cochlea after cisplatin treatment (especially for CtBP2 immunostaining), the most basal locations in the cochlear evaluation we performed were at 420° for CtBP2 and 450° for HC loss. Although ABR threshold shifts after cisplatin insult were observed in both WT and *NOX4*-TG mice, there was no significant difference between WT and *NOX4*-TG mice (Fig. 5B). After cisplatin treatment, OHC loss at 450° in the basal turn was significantly higher in *NOX4*-TG mice than in WT mice (Fig. 5C–D). No IHC loss (at 180° in the apical turn, 270° in the middle turn, and 390° and 450° in the basal turn) was observed in either WT or *NOX4*-TG mice (Fig. 5C–D), which is consistent with data from our group and those of others reporting OHC loss as the primary feature of cisplatin insult (Benkafadar et al., 2017; Mohri et al., 2021; Ramkumar et al., 2021). However, the number of synaptic ribbons in IHCs was significantly lower at 180°, 390°, and 420°, but not 270°, in *NOX4*-TG mice than in WT mice (Fig. 5E–F). These results suggest that the synaptic ribbon is also an earlier target than ABR and IHC loss in ROS-induced DIHL.

3.5. Vulnerability of synaptic ribbons in NOX4-TG mice after noise exposure

Finally, to further examine whether the synaptic ribbon is a target of ROS-mediated acquired SNHL, 2-month-old (adult) WT and *NOX4*-TG mice exposed to intense noise, which induces ROS production in the cochlea (Kurabi et al., 2017). Based on our previous noise exposure experiments using female 5-week-old (young) *NOX4*-TG mice (110 dB sound pressure level [SPL] for 60 min; (Morioka et al., 2018)) and 2-month-old mice (120 dB SPL for 3 h; (Mohri et al., 2021)), in the present study, female WT and *NOX4*-TG mice were exposed to noise (110 dB SPL for 75 min, Fig. 6A), which was a relatively milder level of noise compared to that of our previous study to adult mice (Mohri et al., 2021). Although ABR threshold shifts after noise exposure were observed in both WT and *NOX4*-TG mice, there was no significant difference between WT and *NOX4*-TG mice (Fig. 6B and Fig. S3). OHC loss did not significantly differ between WT and *NOX4*-TG mice, and IHC loss was not observed in either group (Fig. 6C–D). However, the number of synaptic ribbons at 510° in the basal turn, but not at 180°, 270°, 390°, or 450°, was significantly lower in *NOX4*-TG mice than in WT mice (Fig. 6E–F), suggesting that the synaptic ribbon is also an earlier target than ABR and HC loss in ROS-induced NIHL.

4. Discussion

Despite the accumulated evidence for ROS involvement in cochlear HC loss leading to ROS-induced acquired SNHL (Yang et al., 2015), the mechanistic links between ROS and HC loss have not been elucidated. Recently, oxidative stress has been reported to damage cochlear ribbon synapses in cultured cochleae (Zhao et al., 2022). Here, we demonstrated that Piccolo 1, a major component of the ribbon synapse, is a target of ROS. Furthermore, we demonstrated ROS-mediated loss of synaptic ribbons using *NOX4*-TG mice as a live model of ARHL, NIHL, and DIHL. Thus, the synaptic ribbon is a potential therapeutic target in ROS-induced acquired SNHL.

Piccolo is the largest protein (550 kDa) among the main components of the synaptic ribbon, and possesses multiple interactive domains (Butola et al., 2017; Torres and Inestrosa, 2018). In the present study, we showed decreased Piccolo 1 mRNA levels (at P6) and a reduced number of CtBP2 dots in *NOX4*-TG mice compared to those in WT mice (at 1, 4, and 6 months), suggesting that ROS are involved in transcription in synaptic ribbons as well as in their degeneration. Piccolo reportedly functions in SV movement (endocytosis/exocytosis) and modulation of actin dynamics in presynaptic active zones in the nervous system (Torres and Inestrosa, 2018). Additionally, ROS produced by Nox1, Nox2, and Nox4 have been shown to induce the blockage of SV docking and fusion by disrupting actin dynamics (Kang et al., 2020); ROS can also induce SV protein damage and subsequent autophagy of damaged SV (Hoffmann et al., 2019). ROS-mediated functional and pathological damage to SV with close structural interactions with Piccolo may cause synaptic ribbon loss in *NOX4*-TG mice, leading to initial cochlear synaptopathy/hidden hearing loss without HC loss, and finally to acquired SNHL with HC loss.

Although the mechanisms of decreased Piccolo transcription in young (P6) *NOX4*-TG mice remain unknown, ROS are reportedly involved (Milton and Sweeney, 2012; Oswald et al., 2018) in synapse and neuronal development, supporting the developmental delay of synaptic ribbons in *NOX4*-TG mice compared to that in WT mice. The number of synaptic ribbons reached a maximum in 1.5 months *NOX4*-TG mice, especially in males, whereas in WT mice it reached a maximum in 1 month (Fig. 2FB).

C57BL/6 mice (both BL/6 J and BL/6 N strains) are known to show earlier progressive ARHL than other strains owing to the c.723A > G mutation in *cadherin 23*, which causes the degeneration of stereocilia tip links (Kane et al., 2012; Mianne et al., 2016; Noben-Trauth et al., 2003; Yasuda et al., 2020). In these mice, ARHL starts from high- to low-frequency sounds, and SNHL is observed at high-frequency sounds (32 kHz) at 3–6 months of age (Kane et al., 2012; Yasuda et al., 2022). In the present study, the number of CtBP2 dots at 510° gradually decreased from 1 to 6 months in WT mice; however, a significant decrease between 2 and 4 months in *NOX4*-TG mice was observed. In addition, the decrease stopped/plateaued between 4 and 6 months in *NOX4*-TG mice, but not in WT mice. Both C57BL/6 mouse strains possess a *cadherin 23* mutation and show a decrease in synaptic ribbons (Jeng et al., 2020; Peineau et al., 2021). This decrease was shown to be recovered in a C57BL/6 N strain possessing corrected (WT) *cadherin 23* (Jeng et al., 2020). Although the detailed mechanisms of how HC loss is induced by the decrease/degeneration of synaptic ribbons remain unknown, these reports suggest that stereocilia degeneration causes a decrease in synaptic ribbons, finally leading to HC loss and SNHL. A compensatory increase in volume of the remaining synaptic ribbons was also reported in affected mice, suggesting that enlarged synaptic ribbons may exacerbate glutamate release in ribbon synapses, leading to ototoxicity (Jeng et al., 2020; Peineau et al., 2021). The activation of AMP-activated protein kinase is also reportedly involved in the loss of HCs and synaptic ribbons (Hill et al., 2016).

In experiments involving cisplatin insult, significant OHC loss restricted to the basal turn of the cochlea was observed without a corresponding IHC loss. However, the number of synaptic ribbons in IHCs significantly decreased in both the apical and basal turns, but not in the middle turn, in 2-month-old *NOX4*-TG mice. In humans, IHC loss is restricted to the extreme basal region of the aging cochlea, whereas OHC

loss progresses in both the apical and basal ends and selective sparing of mid-cochlear OHCs (Wu et al., 2019). In mice, a basal-to-apical progression of IHC loss, coupled with both apical and basal foci of OHC loss, has been reported in ARHL (Kujawa and Liberman, 2019). These reports support the idea that HCs in the apical and basal turns are more vulnerable than those in the middle turn. Regarding noise exposure experiments, intense noise induced a decrease in Piccolo mRNA transcription in P14/15 WT mice and in the number of CtBP2 dots at only 510° in 2-month-old *NOX4*-TG mice compared with that in WT mice. These results suggest that both intense noise and ROS affect synaptic ribbons at least at the transcriptional level. Considering that several different features of synaptic ribbon decrease after cisplatin (at both apical and basal turns) and intense noise (at only 510° in the basal turn) treatments, intense noise insult may be more similar to the aging effect than cisplatin insult. This is because cisplatin was found to be more toxic or have additional effects on synaptic ribbons compared to those of noise exposure and aging.

5. Conclusions

We found that Piccolo 1 and synaptic ribbons are targets of ROS. Additionally, we demonstrated that ROS are at least one of the causes of cochlear synaptopathy induced by aging (ARHL). Furthermore, we demonstrated that cisplatin and intense noise, both of which induce ROS production (Yang et al., 2015) and aggravate ARHL (Sheffield and Smith, 2019), cause synaptopathy. Thus, protection of synaptic ribbons and reduction in ROS levels are promising approaches to developing novel therapeutic strategies for acquired SNHL.

Funding

This study was supported by Japan Society for the Promotion of Sciences KAKENHI (grant numbers: JP19K22472 and JP21H02672, to TU) and the Takeda Science Foundation (to TU).

CRediT authorship contribution statement

TU had full access to all data from the study and takes responsibility for the integrity of data and accuracy of data analysis. Study conceptualization: TU. Supervision: KT. Investigation: SK, HM, and TU. Formal analysis: SK, HM, and TU. Funding acquisition: TU. Validation: KT and TU. Visualization: SK and TU. Writing of the original draft: TU. All authors reviewed, edited, and approved the final manuscript for publication.

Declaration of Competing Interest

The authors declare that they have no conflicts of interest with the contents of this article.

Data availability

All relevant data are contained within the manuscript and the supporting information.

Acknowledgement

We thank Drs. Chen Lin and Toshiaki Suzuki for their technical assistance with the experimental procedures.

Appendix A. Supplementary data

Supplementary data to this article can be found online at https://doi.org/10.1016/j.nbd.2023.106280.

References

Aedo, C., Aguilar, E., 2020. Cochlear synaptopathy: new findings in animal and human research. Rev. Neurosci. 31, 605–615.
Benkafadar, N., et al., 2017. Reversible p53 inhibition prevents cisplatin ototoxicity without blocking chemotherapeutic efficacy. EMBO Mol. Med. 9, 7–26.
Butola, T., et al., 2017. Piccolo promotes vesicle replenishment at a fast central auditory synapse. Front. Synaptic Neurosci. 9, 14.
Chen, G.D., et al., 2020. Novel oral multifunctional antioxidant prevents noise-induced hearing loss and hair cell loss. Hear. Res. 388, 107880.
Goutman, J.D., et al., 2015. Cochlear hair cells: the sound-sensing machines. FEBS Lett. 589, 3354–3361.
Hickox, A.E., et al., 2017. Translational issues in cochlear synaptopathy. Hear. Res. 349, 164–171.
Hill, K., et al., 2016. Noise-induced loss of hair cells and cochlear synaptopathy are mediated by the activation of AMPK. J. Neurosci. 36, 7497–7510.
Hoffmann, S., et al., 2019. Light-activated ROS production induces synaptic autophagy. J. Neurosci. 39, 2163–2183.
Jeng, J.Y., et al., 2020. Pathophysiological changes in inner hair cell ribbon synapses in the ageing mammalian cochlea. J. Physiol. Lond. 598, 4339–4355.
Kane, K.L., et al., 2012. Genetic background effects on age-related hearing loss associated with Cdh23 variants in mice. Hear. Res. 283, 80–88.
Kang, Y., et al., 2020. Oxidation of reduced graphene oxide via cellular redox signaling modulates actin-mediated neurotransmission. ACS Nano 14, 3059–3074.
Kantardzhieva, A., et al., 2012. Protein composition of immunoprecipitated synaptic ribbons. J. Proteome Res. 11, 1163–1174.
Krey, J.F., et al., 2020. Mechanotransduction-dependent control of stereocilia dimensions and row identity in inner hair cells. Curr. Biol. 30 (442–454), e7.
Kujawa, S.G., Liberman, M.C., 2009. Adding insult to injury: cochlear nerve degeneration after "temporary" noise-induced hearing loss. J. Neurosci. 29, 14077–14085.
Kujawa, S.G., Liberman, M.C., 2019. Translating animal models to human therapeutics in noise-induced and age-related hearing loss. Hear. Res. 377, 44–52.
Kurabi, A., et al., 2017. Cellular mechanisms of noise-induced hearing loss. Hear. Res. 349, 129–137.
Leto, T.L., et al., 2009. Targeting and regulation of reactive oxygen species generation by Nox family NADPH oxidases. Antioxid. Redox Signal. 11, 2607–2619.
Liu, W., et al., 2021. A combined genome-wide association and molecular study of age-related hearing loss in *H. sapiens*. BMC Med. 19, 302.
Ma, M.W., et al., 2017. NADPH oxidase in brain injury and neurodegenerative disorders. Mol. Neurodegener. 12, 7.
Mianne, J., et al., 2016. Correction of the auditory phenotype in C57BL/6N mice via CRISPR/Cas9-mediated homology directed repair. Genome Med. 8, 16.
Milton, V.J., Sweeney, S.T., 2012. Oxidative stress in synapse development and function. Dev. Neurobiol. 72, 100–110.
Mohri, H., et al., 2021. Nox3-derived superoxide in cochleae induces sensorineural hearing loss. J. Neurosci. 41, 4716–4731.
Morioka, S., et al., 2018. Hearing vulnerability after noise exposure in a mouse model of reactive oxygen species overproduction. J. Neurochem. 146, 459–473.
Morioka, S., et al., 2020. Congenital hearing impairment associated with peripheral cochlear nerve dysmyelination in glycosylation-deficient muscular dystrophy. PLoS Genet. 16, e1008826.
Mukherjea, D., et al., 2010. Transtympanic administration of short interfering (si)RNA for the NOX3 isoform of NADPH oxidase protects against cisplatin-induced hearing loss in the rat. Antioxid. Redox Signal. 13, 589–598.
Muller, U., Barr-Gillespie, P.G., 2015. New treatment options for hearing loss. Nat. Rev. Drug Discov. 14, 346–365.
Narui, Y., et al., 2009. Development of distortion product otoacoustic emissions in C57BL/6J mice. Int. J. Audiol. 48, 576–581.
Noben-Trauth, K., et al., 2003. Association of cadherin 23 with polygenic inheritance and genetic modification of sensorineural hearing loss. Nat. Genet. 35, 21–23.
Oswald, M.C.W., et al., 2018. Regulation of neuronal development and function by ROS. FEBS Lett. 592, 679–691.
Peineau, T., et al., 2021. Synaptic release potentiation at aging auditory ribbon synapses. Front. Aging Neurosci. 13, 756449.
Ramkumar, V., et al., 2021. Oxidative stress and inflammation caused by cisplatin ototoxicity. Antioxidants (Basel). 10.
Rousset, F., et al., 2020. Redox activation of excitatory pathways in auditory neurons as mechanism of age-related hearing loss. Redox Biol. 30, 101434.
Schmitz, F., 2009. The making of synaptic ribbons: how they are built and what they do. Neuroscientist. 15, 611–624.
Sheffield, A.M., Smith, R.J.H., 2019. The Epidemiology of Deafness. Cold Spring Harb Perspect Med, p. 9.
Tavanai, E., Mohammadkhani, G., 2017. Role of antioxidants in prevention of age-related hearing loss: a review of literature. Eur. Arch. Otorhinolaryngol. 274, 1821–1834.
Torres, V.I., Inestrosa, N.C., 2018. Vertebrate presynaptic active zone assembly: a role accomplished by diverse molecular and cellular mechanisms. Mol. Neurobiol. 55, 4513–4528.
Ueyama, T., et al., 2014. Maintenance of stereocilia and apical junctional complexes by Cdc42 in cochlear hair cells. J. Cell Sci. 127, 2040–2052.
Ueyama, T., et al., 2016. Constitutive activation of DIA1 (DIAPH1) via C-terminal truncation causes human sensorineural hearing loss. EMBO Mol. Med. 8, 1310–1324.
Ueyama, T., et al., 2020. Rac-dependent signaling from keratinocytes promotes differentiation of intradermal white adipocytes. J. Invest. Dermatol. 140 (75–84), e6.
Wei, M., et al., 2020. Protection of cochlear ribbon synapses and prevention of hidden hearing loss. Neural Plast. 2020, 8815990.

Wu, P.Z., et al., 2019. Primary neural degeneration in the human cochlea: evidence for hidden hearing loss in the aging ear. Neuroscience. 407, 8–20.
Wu, P.Z., et al., 2020. Age-related hearing loss is dominated by damage to inner ear sensory cells, not the cellular battery that powers them. J. Neurosci. 40, 6357–6366.
Yang, C.H., et al., 2015. Age-related hearing impairment and the triad of acquired hearing loss. Front. Cell. Neurosci. 9, 276.
Yasuda, S.P., et al., 2020. C.753A>G genome editing of a Cdh23(ahl) allele delays age-related hearing loss and degeneration of cochlear hair cells in C57BL/6J mice. Hear. Res. 389, 107926.
Yasuda, S.P., et al., 2022. Two loci contribute to age-related hearing loss resistance in the Japanese wild-derived inbred MSM/Ms mice. Biomedicines. 10.
Zhao, C., et al., 2022. SIRT3-mediated deacetylation protects inner hair cell synapses in a H_2O_2-induced oxidative stress model in vitro. Exp. Cell Res. 418, 113280.